The International Journal of Advanced Manufacturing Technology (2018) 96:3251–3262
https://doi.org/10.1007/s00170-018-1715-5

ORIGINAL ARTICLE

Ductile-brittle transition behavior in the ultrasonic vibration-assisted internal grinding of silicon carbide ceramics

Jianguo Cao [1,2] **· Meng Nie** [1,2] **· Yueming Liu** [1,2] **· Jianyong Li** [1,2]

Received: 28 July 2017 / Accepted: 5 February 2018 / Published online: 2 March 2018

Abstract
Silicon carbide (SiC) ceramics play a key role in various engineering applications due to their desirable properties, however, they are typical hard-brittle materials and famous for their poor machinability. Ultrasonic-assisted grinding, a processing method hybridizing the conventional grinding and ultrasonic vibration (UV) machining, is employed as the one applicable machining method for hard-brittle materials. This study focuses on internal grinding of SiC ceramics with the assistance of the UV, and its ductile-brittle transition behavior in the grinding process were investigated experimentally. Following the processing principal of internal grinding and UV machining (i.e., UV-assisted internal grinding, UVAIG), the UVAIG experiment rig were constructed. Conventional internal grinding (CIG) tests, i.e., internal grinding without UV, were also performed on the constructed rig for comparison. In addition, the grinding force and the grinding chips variation behavior with the UV amplitude were also investigated to explore the ductile-brittle transition mechanism in UVAIG. The experiment results evidence that (1) ductile mode grinding is easily achieved in UVAIG, and the critical depth of the cut is deeper in UVAIG than that in CIG, i.e., 0.072 μm in CIG and 0.093 μm in UVAIG; (2) increasing of the critical depth of cut in UVAIG is likely owing to the lower grinding force in UVAIG than that in CIG; and (3) the ultrasonic vibration acted on the axis of the grinding wheel helps in the removal of material on the work-surface, but decreases the grinding energy in the ductile-brittle transition.

Keywords Silicon carbide ceramics · Ultrasonic-assisted grinding · Ductile-brittle transition behavior · Grinding force · Force reduction mechanism

1 Introduction

Until now, mechanical precision components with internal cylindrical surface, such as outer and/or inner races of bearings, injection nozzles for automotive engine, and sleeve mold for small glass lenses, have been widely used in various engineering applications [1, 2]. Ceramics, especially, silicon carbide (SiC) ceramics is an ideal material for components with internal cylindrical surface that used in a high temperature and pressure environment, owing to its desirable material properties that are superior to those of other materials. On the other hand, SiC ceramics is considered as a difficult-to-machine material because of its high brittle and hardness properties [3, 4]. Currently, conventional internal grinding (CIG) is a major method used for precision machining the mechanical components with internal surface, especially for SiC ceramics molding dies [5]. However, there are some problems in CIG of SiC ceramics have been elucidated, e.g., the frequent occurrence of the grinding wheel loading, severe surface cracks and sub-surface damage, and quick grinding wheel wear, thus, it is hard to get a high precision internal surface [6].

Ultrasonic-assisted grinding (UVG), a processing method combining the conventional grinding and ultrasonic vibration (UV) machining, has been introduced as a method to carry out UV-assisted internal grinding (UVAIG) of difficult-to-machine materials. Kumabe et al. found that improved grinding efficiency and reduced grinding forces were reduced in UVAIG of aluminum, copper, and steel compared to those in CIG [7, 8]. Wu et al. performed UVAIG for the internal grinding of stainless steel and experiment results showed that the tangential and normal forces in UVAIG were 70 and 65%

✉ Jianguo Cao
jgcao@bjtu.edu.cn

[1] School of Mechanical, Electronic and Control Engineering, Beijing Jiaotong University, Beijing 100044, China

[2] Key Laboratory of Vehicle Advanced Manufacturing, Measuring and Control Technology, Ministry of Education, Beijing 100044, China

smaller than those in CIG, respectively [9]. Fujimoto et al. demonstrated that the surface roughness, the normal and tangential grinding forces in UVAIG of tungsten decreased by 53, 11, and 41%, compared to those in CIG [10]. In our previous study on grinding characteristics of UVAIG of SiC ceramics [1], we found that that grinding forces in UVAIG were also obviously reduced relative to those in CIG. Additionally, a high accuracy of surface roughness and form accuracy were achieved in UVAIG.

To obtain a high surface quality, hard-brittle materials should be grinded in the ductile mode, i.e., materials are elastically or/and plastically removed in grinding process, finally there are no post-processing are necessary after grinding. In grinding, if the depth of cut is smaller than a critical depth, material in the grinding zone is removed in a shearing likes that in metal cutting due to microscopic plasticity [11]. Therefore, the determination of the critical depth of cut is crucial to achieve the ductile mode grinding. J. Cheng and Y.D. Gong performed single-crystal silicon grinding experiments and found that the material was ductilely removed when critical depth of cut is below 20 nm, and brittlely when the critical depth of cut is deeper than 100 nm [12]. Chen et al. investigated the ductile-brittle transition condition in dynamic grinding. They found that ductile-brittle transition has a strong relation to the micro-hardness of the material, the dynamic fracture toughness, and the coolant and so on [13]. Donald Golini and Stephen D. Jacobs found that the grinding coolant slurry played a key role in ductile-brittle transition in the grinding of ULE (Corning Code 7971Titanium Silicate Low Expansion Glass) [14]. Liang et al. found that the critical depth of cut in UV-assisted scratching (UAS) of monocrystal sapphire is much deeper than that in conventional scratching (CS) without vibration [15]. In our previous study, the critical depth of cut was 0.08 μm in the CS of SiC ceramics to 0.125 μm in UAS, an increase of 56.25% [16].

Although there are many studies on the ductile-brittle transition in the grinding of hard-brittle materials, the ductile-brittle transition phenomenon and mechanism in UAG brittle materials, especially the ductile-brittle transition in UV-assisted grinding of SiC ceramics, have not been fully explored. In this study, the ductile-brittle transition behavior in UVAIG of SiC ceramics was explored by observing the ground work-surfaces, and then the differences between CIG and UVAIG were compared. Furthermore, an ultrasonic-assisted scratching (UAS) of SiC ceramics simulation using a single abrasive grain in UVAIG process was conducted, to provide a comprehensive understanding of physics process in ductile-brittle transition of UVAIG process. At last, the ductile-brittle transition mechanism has been discussed. UVAIG tests were performed on an existing NC internal grinder with an installed ultrasonic spindle. This report describes the design of the tests, the construction of the experimental setup, and the experimental investigations of ductile-brittle transition characteristics in CIG and UVAIG, accompanied by detailed discussions.

2 Ductile-brittle transition nature

2.1 Kinematic characteristics in UVAIG

Figure 1 shows the processing principle of UVAIG. In grinding process, the workpiece and grinding wheel rotate at a speed of n_{w} and n_{g}, respectively; the grinding wheel feeds toward the internal surface at a feed rate of V_{c} in its radial direction. In the meantime, UV vibrates along the axis of the grinding wheel (frequency f, amplitude A_y in y-direction and A_z in z-direction). In addition, the oscillation of the grinding wheel (frequency f_{o}, amplitude A_{o}) helps to expand the grinding surface area.

Grinding is a cutting performance composed by microscopic cutting actions of individual abrasive grains, thus, a better understanding of grain-workpiece interaction is important for reveal the ductile-brittle transition characteristics in UVAIG. The grain-workpiece interactions in UVAIG is schematically given in Fig. 1b, c. In the grinding process, as the ultrasonic vibration is added on the grinding wheel, the abrasive grain on the grinding wheel will engage in a sinusoid movement. The relative motion of the abrasive grains with respect to the workpiece surface generates a removed chip with a sinusoid shape, as shown in Fig. 1c.

Let the global coordinate system be fixed on the workpiece. The origin is the cutting start point in grinding at time $t = 0$, thus, the cutting trajectory of a single abrasive grain in the generated in global coordinate system during UVAIG process can be expressed by Eq. (1).

$$\begin{cases} \mathrm{x}(t) = V_{\mathrm{c}}t + R_{\mathrm{g}}\sin\left(2\pi n_{\mathrm{g}}t\right) \\ y(t) = -A_y\sin(2\pi ft) \\ z(t) = A_y\sin(2\pi ft) + R_{\mathrm{g}} - R_{\mathrm{g}}\cos\left(2\pi n_{\mathrm{g}}t\right) + A_{\mathrm{o}}\sin\left(2\pi f_{\mathrm{o}}t\right) \end{cases} \tag{1}$$

where R_{g} is the grinding wheel radius.

Therefore, Due to the UV in y-direction, the grain moves upward and downward alternatively in the cutting process, leading to the periodic variation of the grain depth of cut (Fig. 2a). Turing to z-direction as shown in Fig. 2b, similar to that in y-direction, the sinusoidal cutting trace of the grain is generated in the xz-plane, owing to the UV of the grain in the z--direction. This indicates that the grinding force of the single abrasive grain will be periodically varied owing to the periodic variation of the grain depth of cut.

Fig. 1 Processing principle of UVAIG

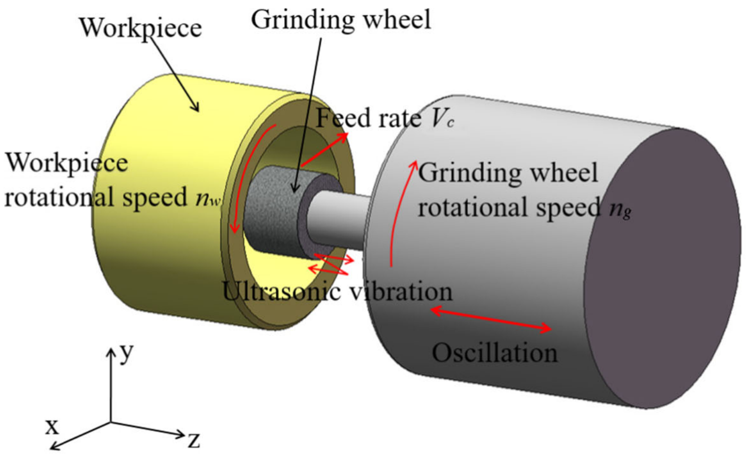

(a) isometric view

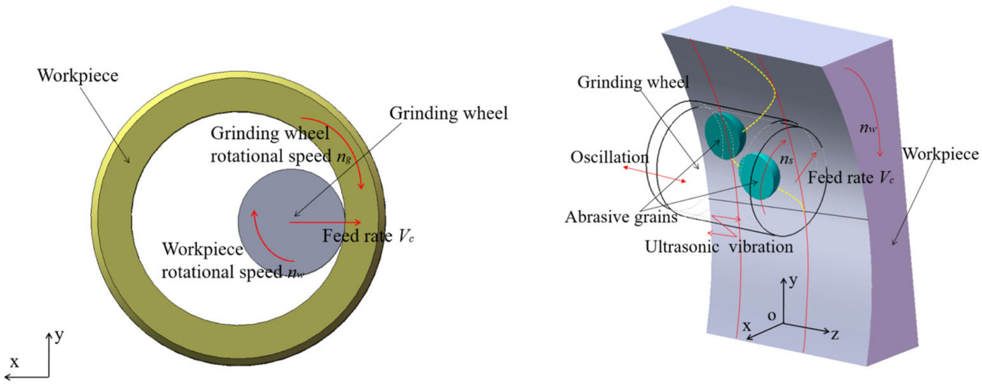

(b) *xy*-plane view (c) single grain-workpiece material interaction

Fig. 2 Cutting trajectory of an abrasive grain in UVAIG process

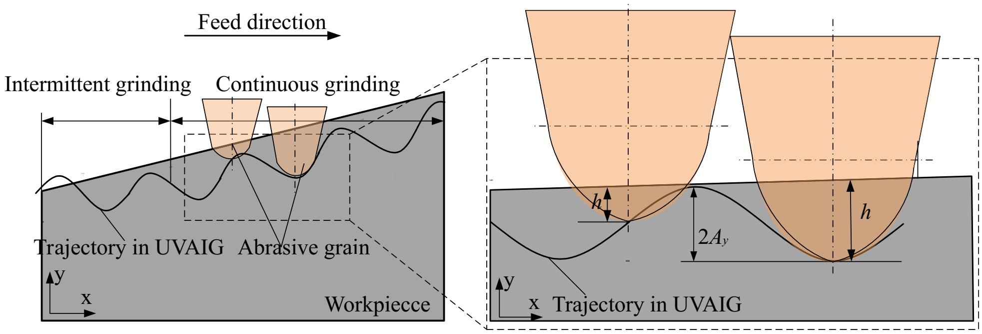

(a) Cutting Trajectory in *xy*-plane

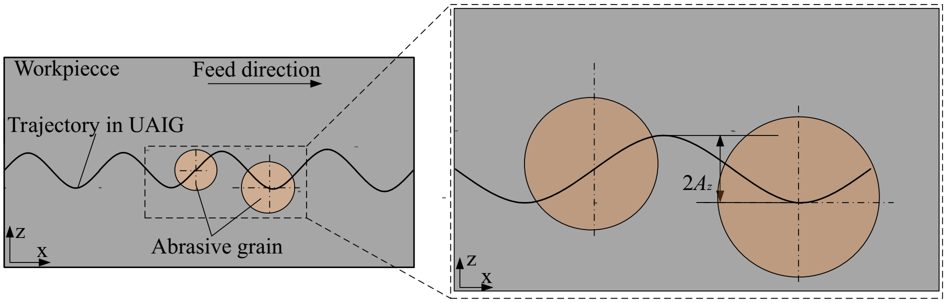

(b) Cutting Trajectory in *xz*-plane

2.2 Grinding force modeling

In grinding, the normal and tangential forces, f_n and f_t, acting on a single abrasive grain depends on the cross-sectional area of the undeformed chip A_{cs} (Fig. 3). According to [17], it is can be expressed as:

$$f_n = kA_{cs} \tag{2}$$

$$f_t = k_1 kA_{cs} \tag{3}$$

where k and k_1 are the chip thickness coefficient and the ratio of the tangential force to the normal force, respectively.

In the grinding process, A_{cs} can be written as [17]:

$$A_{cs} = a_e R_w n_w / c_d R_g n_g L_c \tag{4}$$

where R_w, c_d, a_e, n_w, n_g, and L_c are the workpiece radius, the active cutting edge density, the wheel depth of the cut, the workpiece rotational speed, the grinding wheel rotational speed, and the undeformed chip length, respectively.

Thus, f_n and f_t, acting on the grain in the grinding process can be expressed as:

$$f_n = ka_e R_w n_w / c_d R_g n_g L_c \tag{5}$$

$$f_t = k_1 ka_e R_w n_w / c_d R_g n_g L_c \tag{6}$$

Thus, the grinding force F_n and F_t in the in the grinding process can be expressed as:

$$F_n = Nka_e R_w n_w / c_d R_g n_g L_c \tag{7}$$

$$F_t = Nk_1 ka_e R_w n_w / c_d R_g n_g L_c \tag{8}$$

where N is the total number of active cutting abrasives in grinding zone.

2.3 Ductile-brittle transition in grinding process

In UVAIG process, the arbitrary abrasive grain on the grinding wheel takes part in the cutting action at point P_0 and gets out of the action at point P_1, accordingly, the cutting depth of a single grain increases from zero to maximum g_m together with the cutting force of the abrasive grain f_t and f_n are increased (Fig. 4). The crack mechanism of ceramics material in the grinding process can be described as [18, 19]:

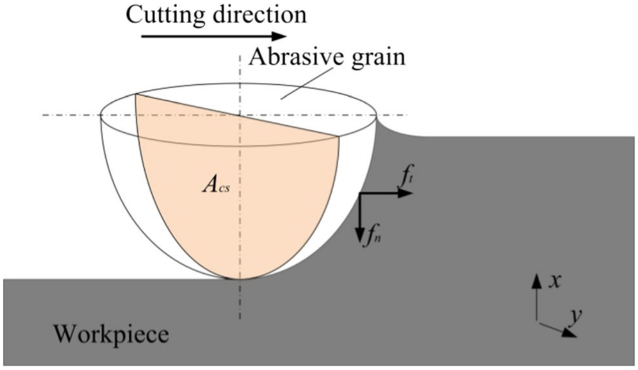

Fig. 3 Schematic illustration of a single abrasive grain cutting force in grinding

(a) At a low grinding force, the abrasive grain plows a groove and the material is removed in plastic deformation, resulting in a sub-surface region with plastically deformed material and a ductile-ground groove;

(b) As the grain continues to travel, the groove depth and plastic deformation zone are increased with the increase of the grinding force, leading to a radical/median crack forms beneath the abrasive grain when the grinding force reaches some critical value;

(c) Lateral cracks occur when the grinding force is bigger than the threshold for median crack formation. The formation and propagation of the lateral cracks facilitates brittle material removal. However, it should be noted that a plastically deformed zone remains though material is removed by crack propagation.

According to the energy conservation law, the energy consumed in ductile mode grinding U_d can be calculated from the cutting velocity and the normal cutting force, thus, it can be written as [20]:

$$U_d = f_n v \tag{9}$$

where f_n is the normal force of an abrasive grain in the grinding, and v is the cutting velocity of the abrasive grain.

As mentioned above, material is removed by crack propagation in brittle-mode grinding, leading to two major types of cracks, i.e., radial/median and lateral cracks. The energy consumed in brittle-mode grinding is expressed below [21]:

$$U_b = (2C_l + 2C_m) v \gamma_s \tag{10}$$

where C_l and C_m are the length of the lateral and radial/median crack, respectively, and γ_s is the surface energy of the material.

In grinding, C_m is determined by fracture toughness and the critical grinding force of fracture [21]:

$$C_m = \left(\frac{4\chi P_c}{K_{IC}} \right)^{2/3} \tag{11}$$

where χ is the geometric constant (0.064 for SiC ceramics) [20], K_{IC} is the fracture toughness, P_c is normal load of an abrasive grain acted in the direction of the radial/median crack, i.e., the normal force of an abrasive grain in the grinding process, here $P_c = f_n$.

In abrasive machining, C_l could be approximately expressed as [21]:

$$C_l \cong \frac{C_m}{7} \tag{12}$$

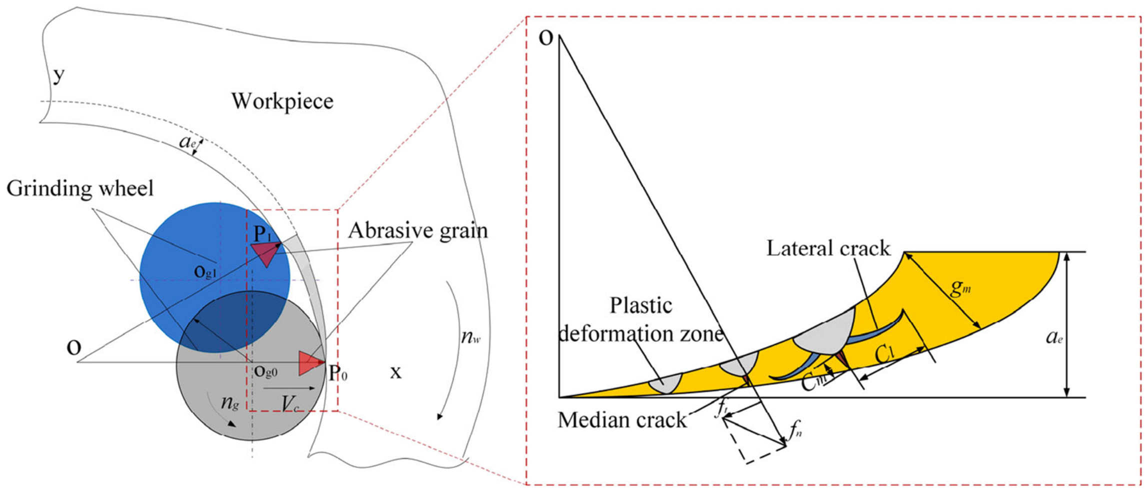

Fig. 4 Crack mechanism of ceramics material in the grinding process

In brittle-mode grinding, the total consumed energy in brittle-mode grinding is given by:

$$U_{\text{total}} = U_{\text{d}} + U_{\text{b}} = (2C_{\text{l}} + 2C_{\text{m}})v\gamma_{\text{s}} + f_{\text{n}}v$$
$$= \frac{16}{7}v\left[\left(\frac{4\chi f_{\text{n}}}{K_{\text{IC}}}\right)^{2/3}\gamma_{\text{s}} + f_{\text{n}}\right] \tag{13}$$

In grinding, if the consumed total energy is transferred into the workpiece material done by the abrasive grain through the cutting event and exceeds its threshold energy for crack initiation U_{l}, the material removal transferred into brittle mode; otherwise, the material is removed in a ductile mode [22, 23]. Therefore, it can be considered that:

If

$$U_{\text{l}} < U_{\text{total}}, \tag{14}$$

the lateral crack and material can be removed by cracks propagation in a brittle grinding mode.

If

$$U_{\text{l}} = U_{\text{total}}, \tag{15}$$

ductile grinding mode allows energy transits into the brittle grinding mode, and the transition point is considered the critical depth of cut.

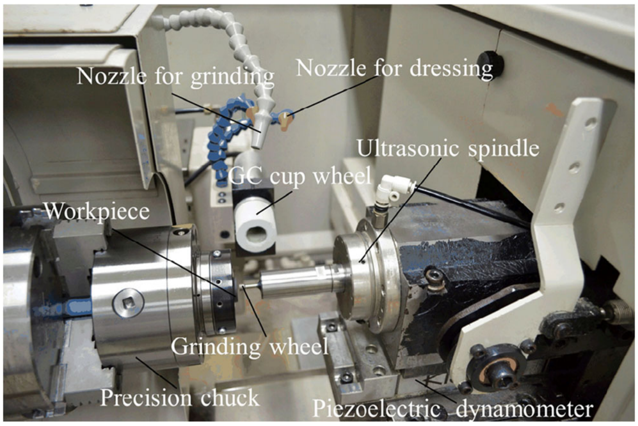

Fig. 5 Experimental setup for UVAIG

3 Experiment and simulation detail

3.1 Experiment setup

UVAIG experiments were performed using a SiC ceramics workpiece that is ϕ12 mm in the inner diameter, ϕ22 mm in the outer diameter, and 13 mm in thickness. Figure 5 shows the constructed experimental setup for UVAIG. An ultrasonic spindle with a diamond grinding wheel screwed onto its the end face (URT40 by Takesho Co., Ltd.) is installed on a commercial NC internal grinder (GRIND-X IGM15EX by Okamoto Machine Tool Works, Ltd.). In the grinding process, the grinding forces are recorded by a 3-component piezoelectric dynamometer (9256A by Kistler Co., Ltd.). In grinding process, the coolant slurry (solution type, 1.6% dilution) is flowed into the grinding zone. The topographies of the

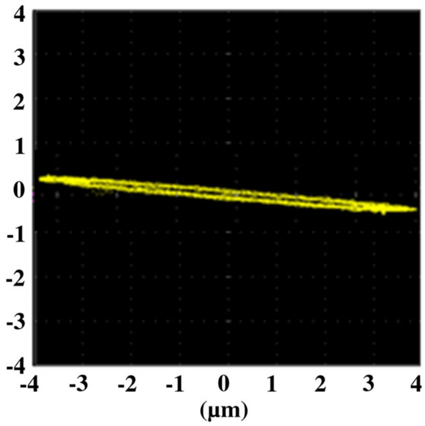

Fig. 6 UV traces of grinding wheel

Table 1 Experiment conditions for the observation of the ductile-brittle transition

No.	Wheel	Workpiece rotational speed n_w (rpm)	Wheel rotational speed n_g (rpm)	Stock removal (μm)	Feed rate V_c (μm/min)	Ultrasonic amplitude (μm)
1	SD400P100M	300	4000	50	10	0/4
2	SD1000P100M	300	3000	50	10	0/4
3	SD1000P100M	300	4000	50	10	0/4
4	SD3000P100M	300	4000	50	10	0/4

work-surface were examined by using a scanning electron microscope (SEM) (ERA-8900S by Elionix Co., Ltd.). The vibration amplitudes of the grinding wheel were measured with a laser Doppler vibrometers (LV-1610 by Ono Sokki Co., Ltd.). The UV amplitudes were 4 μm for the z-axis and 0.25 μm for the y-axis with frequency $f = 40$ kHz (Fig. 6).

3.2 Experimental design

In order to observe the ductile-brittle transition behavior of the SiC ceramics in UVAIG, grinding tests compared with CIG were carried out under different groups of experimental conditions as shown in Table 1.

In grinding, the maximum cutting depth of a single grain g_m is determined by [24]:

$$g_m = 2a\frac{V_w}{V_g}\sqrt{\frac{\Delta}{D_e}} \tag{16}$$

where a is the successive cutting edge spacing, V_w and V_g are the workpiece and the grinding wheel tangential speed, respectively, Δ is the grinding wheel depth of cut, and D_e is the equivalent wheel diameter. In internal grinding, D_e can be written by [24]:

$$D_e = \frac{D_g}{1 - {}^{D_g}/_{D_w}} \tag{17}$$

where D_g and D_w are the grinding wheel and the workpiece diameter, respectively.

Successive cutting edge spacing a is determined by [25]:

$$a = 137.9M^{-1.4}\sqrt[3]{\frac{2\pi}{\eta_g}} \tag{18}$$

where M is the grit number and η_g is the density of the wheel, (%).

Table 2 g_m in different experiment conditions

	No.1	No.2	No.3	No.4
g_m (μm)	0.251 μm	0.093 μm	0.072 μm	0.019 μm

Table 2 shows the gm obtained from Eq. (16)–(18) under the condition as shown in Table 1.

3.3 Simulation detail

In order to simplify the analysis of the grinding wheel-workpiece interaction, the cutting edge shape of the abrasive grain should be approximated by a well-defined geometry. Figure 7 shows the 3D-SEM images of SD1000P100M used for UVAIG. It can be seen that the shapes of the abrasive grains are similar with the tip tops and round bottoms. In this work, the shape of the grains was simplified to a spherical tip just like that proposed by Shaw [26], Sanjay Agarwal [27], and octahedron by DeFu Liu [28].

Figure 8 shows simulation model of the UAS. The grain was defined as rigid part with a vertical angle and nose radius of the grain are 80° and 15 μm, respectively. The workpiece was generated by smoothed particle hydrodynamics method with the geometry of 90 μm × 80 μm × 30 μm. In the scratching process, the bottom of the workpiece was fully constrained. The amplitudes of UV is $A_y = 0.25$ μm in y-direction (the vertical direction relative to the workpiece in the UVAIG) and $A_z = 4$ μm in z-direction (the axis direction of the grinding wheel in the UVAIG), and frequency of $f = 40$ kHz, and feed speed at a speed of $V_c = 0.5$ m/s along the x-direction are added on the grain. For comparison, a conventional scratching (CS) without UV was also performed by moving the tool along on the workpiece at the same speed V_c used in UAS.

4 Results and discussion

4.1 Ductile-brittle transition behavior

Figure 9 shows the SEM images of the work-surface by CIG and UVAIG for different experimental conditions. As shown in Fig. 9a, b, brittle cracks and fractures can be clearly observed in the work-surface both in CIG and UVAIG, indicating that the brittle fracture was predominant material removal mode when $g_m = 0.251$ μm due

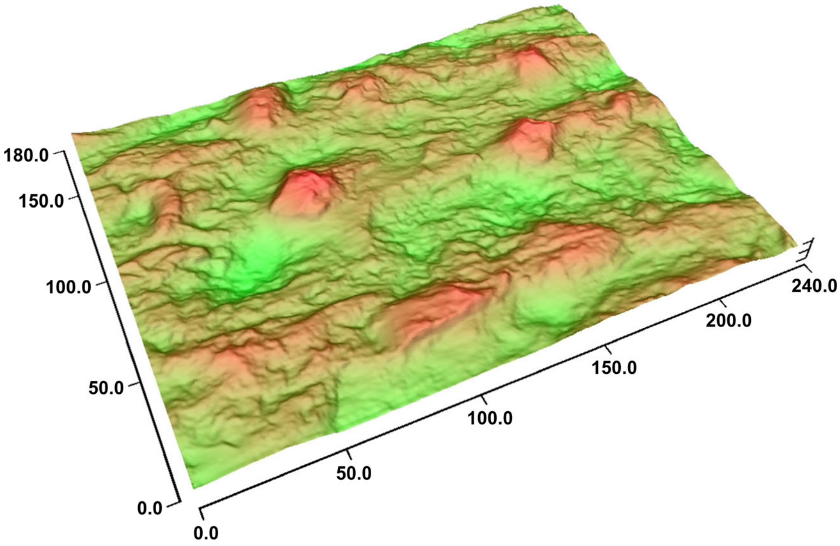

Fig. 7 3D image of SD400P100M grinding wheel

to the cooperative action of the shear stress and high compressive stress [29]. When $g_m = 0.093$ μm, obvious macro-brittle fractures and cracks were also generated in the work-surface formed by CIG (Fig. 9c). Unlike that in CIG, a smooth surface outside of the cracks and macro-brittle fractures that are formed in the work-surface by UVAIG, indicating that a ductile-brittle transition occurred when $g_m = 0.093$ μm (Fig. 9d).

However, as observed in Fig. 9e, a smooth surface near the macro-brittle fractures and cracks formed in the work-surface formed by CIG when $g_m = 0.072$ μm. In contrast, although some cracks can be observed in the work-surface, almost of the work-surface was smooth in UVAIG when $g_m = 0.072$ μm (Fig. 9f), indicating that the grinding mode was predominantly ductile. Considering the images in Fig. 9g, h, almost all of the work-surface was smooth both in CIG and UVAIG, suggesting that the grinding mode was predominantly ductile when $g_m = 0.019$ μm.

Therefore, the ductile-brittle transition occurs at $g_m = 0.072$ μm in CIG, and at $g_m = 0.093$ μm in UVAIG. This means that the critical depth of cut (ductile-brittle transition depth) is increased in UVAIG compared with that in CIG, and ductile mode grinding is more easily achieved in UVAIG (Fig. 10). These consistent with the experimental observations carried out by Liang et al. [15], Cao et al. [16], and Chen et al. [30]., in UAS of single-crystal silicon, SiC ceramics, and UAG of silicon, respectively.

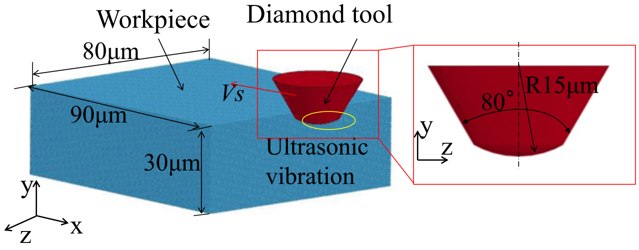

Fig. 8 Simulation model

4.2 Grinding force behavior

The grinding force is an indicator parameter to characterize the material removal mode. The grinding force in the grinding processes were plotted in Fig. 11. It can be found from Fig. 11 that both the tangential force F_t and the normal force F_n either in CIG or UVAIG increased with increasing of g_m. It was interesting that the values for both the F_n or F_t in UVAIG were much smaller than those in CIG. Particularly, the grinding F_n and F_t are 10 N and 3 N in UVAIG and 15 N and 5 N in CIG at $g_m = 0.072$ μm, while F_n and F_t are 15 and 3.5 N in UVAIG and 18 and 6 N in CIG at $g_m = 0.093$ μm. Because the grinding force in UVAIG is smaller than that in CIG, it is deduced from Eq. (13) that the total grinding energy consumed in brittle-mode grinding U_{total} in UVAIG is smaller than that in CIG.

Considering again the data presented in Fig. 11, the normal force in CIG at $g_m = 0.072$ μm was almost equal to that in UVAIG at 0.093 μm. At $g_m = 0.072$ μm, a ductile-brittle transition occurs in CIG because the total energy consumed in the brittle-mode grinding exceeds its threshold energy for brittle crack initiation. However, because the normal force f_n in UVAIG is smaller than that in CIG, the total energy consumed in the brittle-mode grinding is lower than the threshold energy for crack initiation, resulting in UVAIG remaining in ductile grinding mode. As the grinding force increased at $g_m = 0.093$ μm, CIG totally transferred into brittle grinding mode. The ductile-brittle transition occurred in UVAIG because to the total

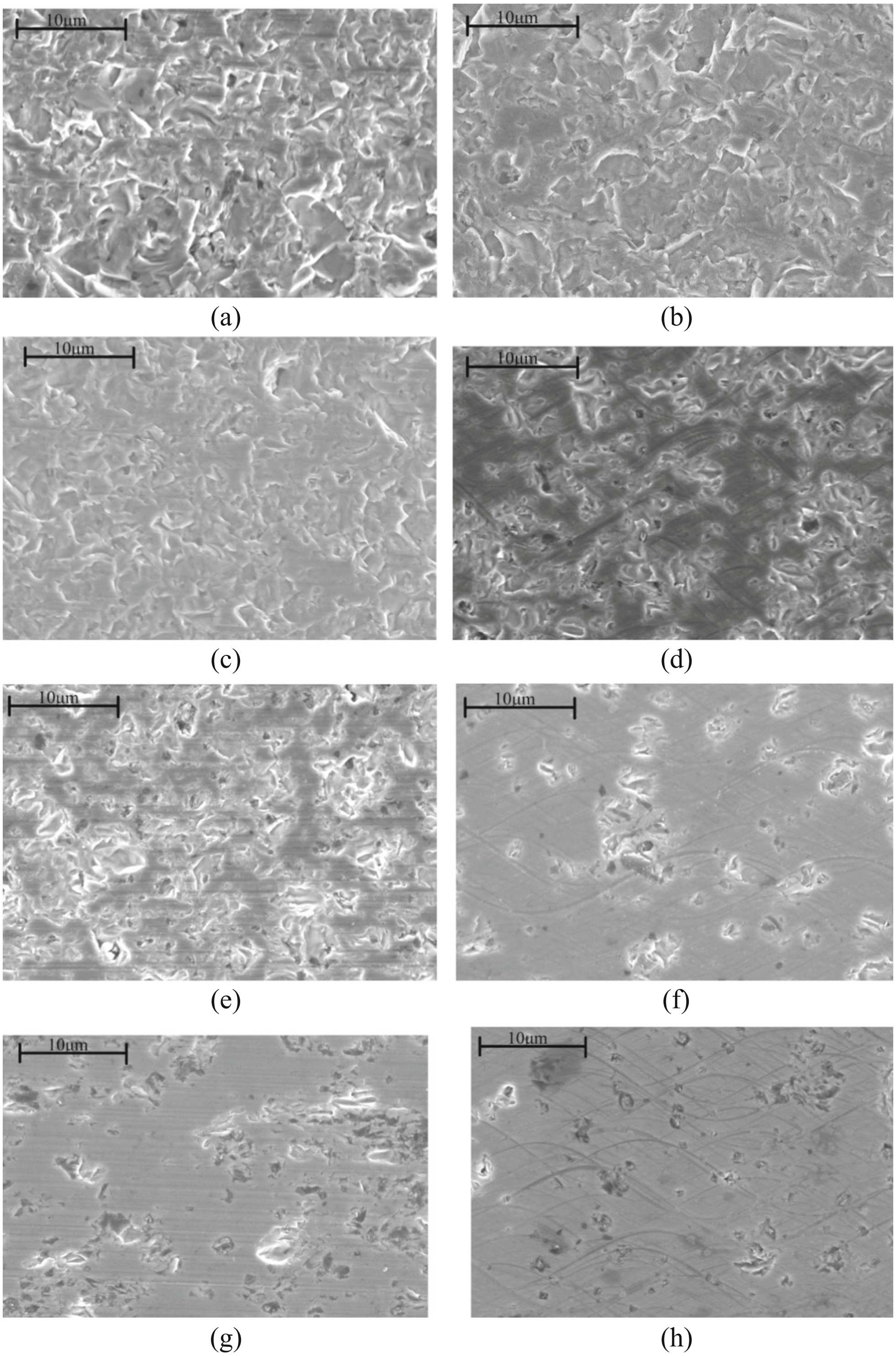

(a) (b) (c) (d) (e) (f) (g) (h)

Fig. 9 Work-surface by CIG and UVAIG at different experimental conditions. **a** Work-surface integrity by CIG at g_m = 0.251 μm. **b** Work-surface integrity by UVAIG at g_m = 0.251 μm. **c** Work-surface integrity by CIG at g_m = 0.093 μm. **d** Work-surface integrity by UVAIG at g_m = 0.093 μm. **e** Work-surface integrity by CIG at g_m = 0.072 μm. **f** Work-surface integrity by UVAIG at g_m = 0.072 μm. **g** Work-surface integrity by CIG at g_m = 0.019 μm. **h** Work-surface integrity by UVAIG at g_m = 0.019 μm

grinding energy consumed in brittle-mode grinding exceeded the threshold energy for brittle crack initiation. Chen et al. [30] carried out an experimental and theoretical research on UV grinding of silicon. Results showed that the grinding energy in ductile mode in UVG is smaller than that in conventional grinding. Zhou et al. [31] also found that the specific cutting energies decreased with the cutting depth in UAG of BK7 optical glass. Therefore, it is also concluded that the critical depth of cut is increased in UVAIG compared with that in CIG is due to the decreased grinding force in UVAIG relative to that in CIG, finally leading to the grinding energy consumed in brittle-mode grinding being smaller than that in CIG.

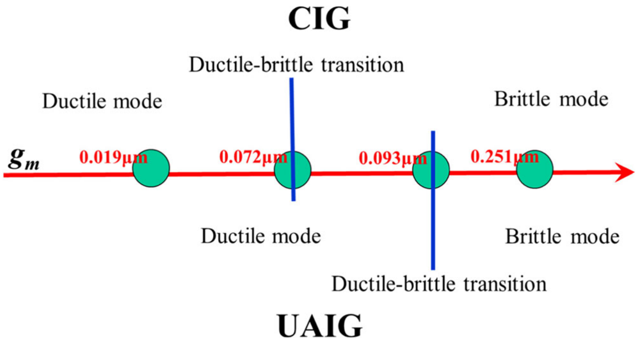

Fig. 10 Illustration of ductile-brittle transition in CIG and UVAIG

As discussed above, the grinding force, especially the normal force, has a direct influence on the ductile-brittle transition. It is inferred from Eqs. (2) and (3) that the larger cross-sectional area A_{cs} is, the larger value of the grinding forces become. The grinding forces in UVAIG are lower than that in CIG is also likely due to the smaller A_{cs} in UVAIG relative to that in CIG. If this is correct, the cross-sectional area of the chips formed in UVAIG ought to be smaller than those in CIG. To confirm this hypothesis, the chips formed both in UVAIG and in CIG of SiC ceramics were gathered under the condition $g_m = 0.251$ µm with a UV amplitude A that changed from 4 to 0 µm. The cross-sectional profiles of the chips were observed by a 3D-SEM. The cross-sectional area was calculated by measuring the depths and widths of the chips.

Figure 12 shows the SEM images of chips formed in UVAIG and CIG, and Fig. 13 shows the variation of the cross-sectional area of the chips formed in UVAIG and CIG as measured by 3D-SEM. The mean cross-sectional area of the chips became smaller with the increasing of UV amplitude A, accordingly, the grinding force also decreased with the increasing of UV amplitude A (Fig. 14). Therefore, it is concluded that a significant decreasing of grinding force primarily due to the great reduction of mean cross-sectional area of the chips in UVAIG compared to that in CIG.

4.3 Physics process

The cutting depth g_m of the UAS and CS in this work are set to be 0.093 µm to investigate the physics process in UCAIG and CIG. It is widely accepted that knowledge of stress states during the cutting process is key to understanding material removal mechanism [32]. The effective stress field on the cross surface along the cutting direction during the UAS and CS processes were investigated (Fig. 15).

When the grain is cutting into the workpiece, considerable stress is generated in the area around the grain and in the sub-surface underneath the grain. In the CS process, the stress fields are basically stabilized after the grain cuts entirely into the workpiece both in the cross surface and the top surface. Turing to the UAS process, it is observed that the stress fields are un-continuous, owing to the ultrasonic vibrates in y-direction and its amplitude is larger than the g_m. Further, it is also observed that the stress fields on both surfaces suddenly expand further at 18.75 µs (Fig. 15g) and also become wider at 25 µs than those in the CS process (Fig. 15c,

Fig. 11 Maximum cutting depth g_m versus the grinding force

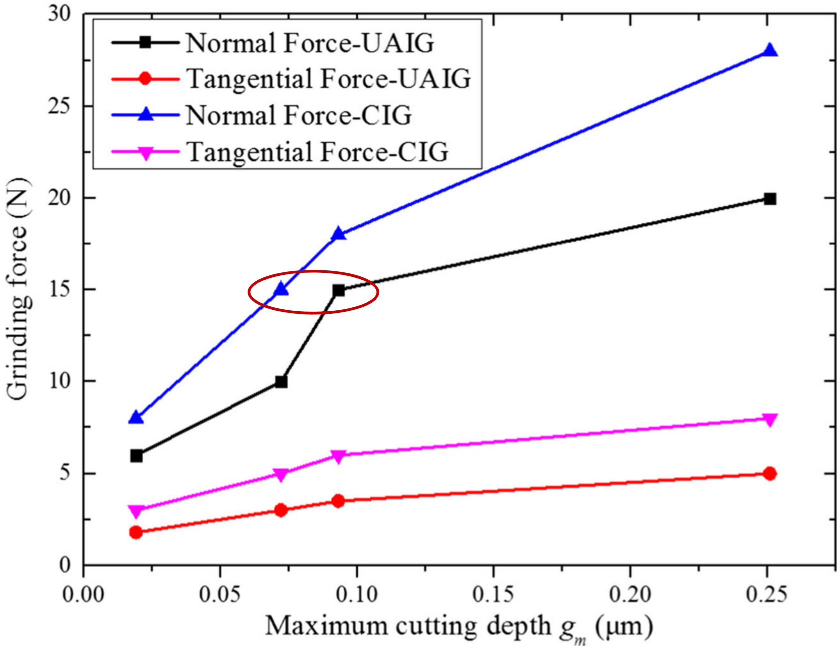

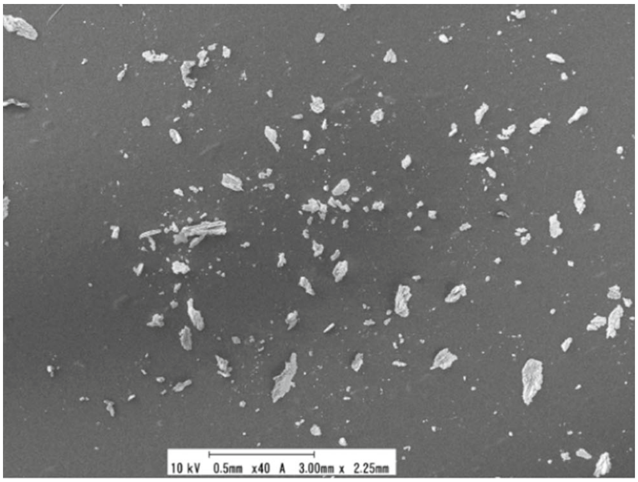

(a) A=4μm

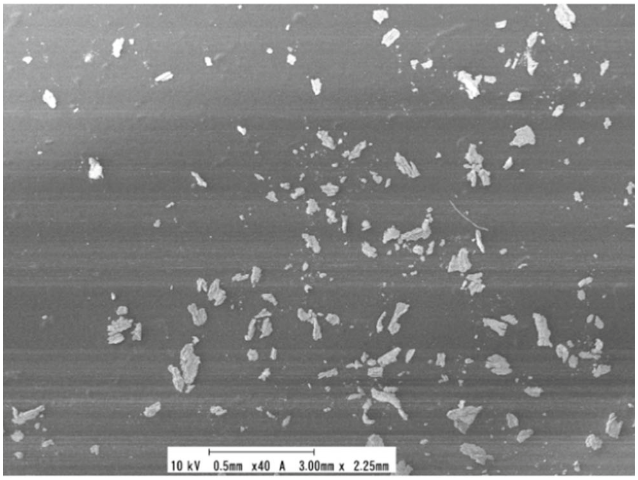

(b) A=2μm

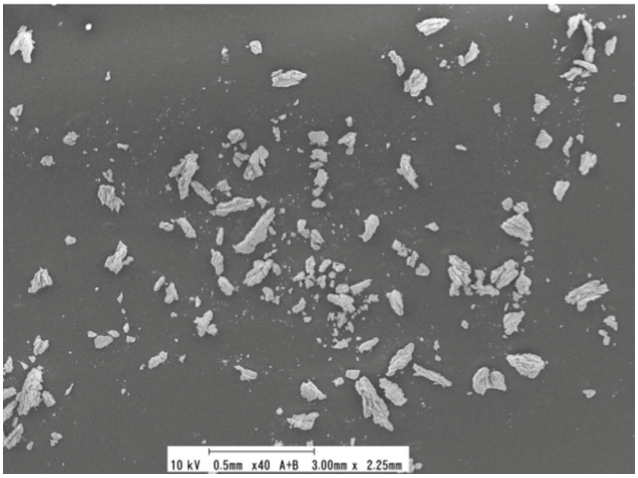

(c) A=0μm

Fig. 12 Chips formed in CIG and UVAIG

g). These are attributed to the impact arising from the UV against the workpiece.

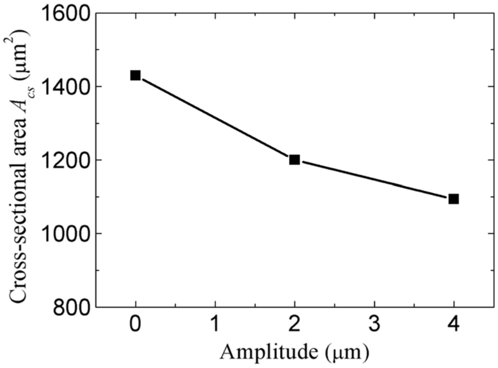

Fig. 13 Cross-sectional area *Acs* versus amplitude *A*

In the grinding process, UV vibrates along the axis of the grinding wheel, leading to engagement of the abrasive grain in a sinusoid movement (as shown in Figs. 9d, 6f, and 6h), generating a removed chip with a sinusoid shape. This leads to a longer undeformed chip length L_c in UVAIG compared to that in CIG, eventually reducing the grinding force in UVAIG relative to that in CIG (as mentioned in Eq. (4), a longer L_c results in a smaller A_{cs} of the chips). On the other hand, due to the UV of the grain vibrates in axis directions of the grinding wheel (*z*-direction in UAS), not only does the grain motion direction change, but also the grinding energy changes in the material removal process. The grinding energy from UV is released and acts on the workpiece, leading to the impact of the grain on the workpiece in the *z*-directions. Upon impact of the grain on the workpiece, the stress field spreads from the impact site, benefiting in the removal of material on the work-surface (Fig. 15). As a consequence, a large portion of the grinding energy consumed in the material removal process on the work-surface, resulting in a

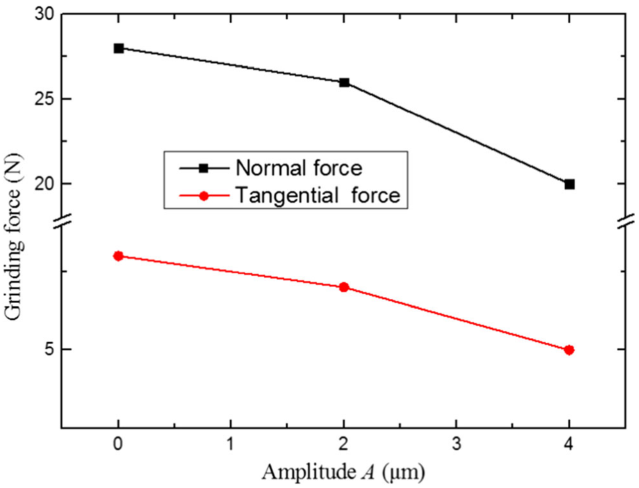

Fig. 14 Grinding force versus the amplitude *A*

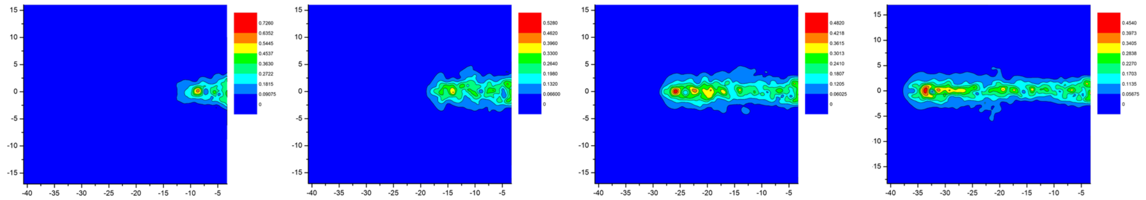

(a) Time=6.25μs, CS (b) Time=12.5μs, CS (c) Time=18.75μs, CS (d) Time=25μs, CS

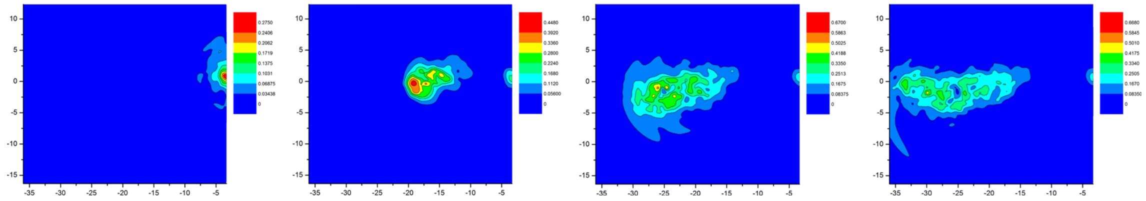

(e) Time=6.25μs, UAS (f) Time=12.5μs,UAS (g) Time=18.75μs, UAS (h) Time=25 μs, UAS

Fig. 15 Effective stress distribution on the work-surface

significant reduction of the grinding energy consumed in brittle-mode grinding. Finally, the critical depth of cut is increased in UVAIG compared with that in CIG.

5 Conclusion

To understand ductile-brittle transition behavior in the ultrasonic vibration assisted internal grinding (UVAIG) of SiC ceramics, an UVAIG test was performed on a SiC ceramic sample using an in-house-produced experimental setup. The ductile-brittle transition behavior in the UVAIG test was compared to that in the conventional internal grinding (CIG) test without ultrasonic vibration. The results and conclusions can be summarized as follows:

(1) The ductile-brittle transition occured at $g_m = 0.072$ μm in CIG and at $g_m = 0.093$ μm in UVAIG, meaning that critical depth of cut was increased in UVAIG compared with that in CIG, thus, ductile mode grinding was more easily achieved in UVAIG.

(2) The ultrasonic vibration amplitude results in a significant reduction of grinding force primarily due to the great influence upon mean cross-sectional area of the chips. Additionally, the grinding force in UVAIG decreases the total energy consumed in brittle-mode grinding.

(3) The investigations of the stress distribution on the work-surface of the workpiece along the cutting direction show that the stress fields becomes wider in the UAS process than in the CS process because of the impact arising from the ultrasonic vibration. Thus, the ultrasonic vibration acted on the axis of the grinding wheel helps in the removal of material on the work-surface, but decreases the grinding energy in the ductile-brittle transition.

Acknowledgments The authors would like to thank the support of the National Natural Science Foundation of China (No.51605024). The present work was also supported by the Fundamental Research Funds for the Central Universities (M17RC00020).

References

1. Cao J, Wu Y, Lu D, Fujimoto M, Nomura M (2014) Fundamental machining characteristics of ultrasonic assisted internal grinding of SiC ceramics. Mater Manuf Processes 29:557–563
2. Kanai K, Sugiyama K, Shiotani E, Nishimura K, Uchiyama J, Suzuki K, Inomata J, et al. (2010) Cylindrical internal surface with thermally spray coating
3. Shigeyuki Sömiya YI (2009) Silicon carbide ceramics-1 fundamental and solid reaction. Springer, Netherlands
4. Hall C, Tricard M, Murakoshi H, Yoko H (2005) New mold manufacturing techniques. Proc SPIE—Int Soc Optical Eng 5868: 58680V
5. Agarwal S, Rao PV (2013) Predictive modeling of force and power based on a new analytical undeformed chip thickness model in ceramic grinding. Int J Mach Tool Manu 65:68–78
6. Nomura M. (2007) Study of ultrasonic vibration assisted internal grinding of small holes. Doctoral Dissertation Sendai, Japan: Tohoku University. (In Japanese)
7. Kumabe J (1961) Study on ultrasonic internal grinding by using the longitudinally vibrated grinding wheel: 1st report, traverse ultrasonic cutting. Trans Japan Soc Mech Eng 27:1404–1411
8. Kumabe J, Ito Y (1961) Study on ultrasonic internal grinding by using the longitudinally vibrated grinding wheel: 2nd report, the outline of the effects. Trans Japan Soc Mech Eng 27:1412–1418
9. Wu Y, Nomura M, Kato M, Tachibana T (2003) Study of internal ultrasonic vibration assisted grinding of small holes: construction of ultrasonic vibration spindle and its fundamental performances. J Japan Soc Grinding Eng 47:550–555
10. Fujimoto M, Wu Y, Cao J. High precision ultrasonically assisted internal grinding (uaig) of difficult-to-machining materials using

metal bonded diamond wheels: Proceedings of International Conference on Leading Edge Manufacturing in 21st century : LEM21, 2011[C]

11. Zhang X, Arif M, Liu K, Kumar AS, Rahman M (2013) A model to predict the critical undeformed chip thickness in vibration-assisted machining of brittle materials. Int J Mach Tool Manu 69:57–66
12. Cheng J, Gong YD (2014) Experimental study of surface generation and force modeling in micro-grinding of single crystal silicon considering crystallographic effects. Int J Mach Tool Manu 77:1–15
13. Chen M, Zhao Q, Dong S, Li D (2005) The critical conditions of brittle–ductile transition and the factors influencing the surface quality of brittle materials in ultra-precision grinding. J Mater Process Tech 168:75–82
14. Golini D, Jacobs SD. Transition between brittle and ductile mode in loose abrasive grinding: San Dieg - DL Tentative, 1990[C]
15. Liang Z, Wang X, Wu Y, Xie L, Jiao L, Zhao W (2013) Experimental study on brittle–ductile transition in elliptical ultrasonic assisted grinding (EUAG) of monocrystal sapphire using single diamond abrasive grain. Int J Mach Tool Manu 71:41–51
16. Cao J, Wu Y, Lu D, Fujimoto M, Nomura M (2014) Material removal behavior in ultrasonic-assisted scratching of SiC ceramics with a single diamond tool. Int J Mach Tool Manu 79:49–61
17. Cao J, Wu Y, Li J, Zhang Q (2015) A grinding force model for ultrasonic assisted internal grinding (UAIG) of SiC ceramics. Int J Adv Manuf Technol 81:875–885
18. Cheng J, Yin G, Wen Q, Song H, Gong Y (2015) Study on grinding force modelling and ductile regime propelling technology in micro drill-grinding of hard-brittle materials. J Mater Process Technol 223:150–163
19. Wang Y, Lin B, Wang S, Cao X (2014) Study on the system matching of ultrasonic vibration assisted grinding for hard and brittle materials processing. Int J Mach Tool Manu 77:66–73
20. Arif M, Zhang X, Rahman M, Kumar S (2013) A predictive model of the critical undeformed chip thickness for ductile–brittle transition in nano-machining of brittle materials. Int J Mach Tool Manu 64:114–122
21. Bifano TG, Fawcett SC (1991) Specific grinding energy as an in-process control variable for ductile-regime grinding. Precis Eng 13: 256–262
22. Slikkerveer PJ, Bouten PCP, Veld FHI, Scholten H (1998) Erosion and damage by sharp particles. Wear 217:237–250
23. Zarepour H, Yeo SH (2012) Predictive modeling of material removal modes in micro ultrasonic machining. Int J Mach Tool Manu 62: 13–23
24. Marinescu ID.(2006) Handbook of machining with grinding wheels. CRC, Taylor & Francis,
25. Zhou X, Xi F (2002) Modeling and predicting surface roughness of the grinding process. Int J Mach Tool Manu 42:969–977
26. Shaw. (1972) New developments in grinding. Proceedings of the international grinding conference, Pittsburgh, Pennsylvania, April 18–20, 1972
27. Agarwal S, Rao PV (2012) Predictive modeling of undeformed chip thickness in ceramic grinding. Int J Mach Tool Manu 56:59–68
28. Liu D, Cong WL, Pei ZJ, Tang Y (2012) A cutting force model for rotary ultrasonic machining of brittle materials. Int J Mach Tools Manuf 52:77–84
29. Ghosh D, Subhash G, Radhakrishnan R, Sudarshan TS (2008) Scratch-induced microplasticity and microcracking in zirconium diboride–silicon carbide composite. Acta Mater 56:3011–3022
30. Chen JB, Fang QH, Wang CC, Du JK, Liu F (2016) Theoretical study on brittle–ductile transition behavior in elliptical ultrasonic assisted grinding of hard brittle materials. Precis Eng 46:104–117
31. Zhou M, Zhao P (2016) Prediction of critical cutting depth for ductile-brittle transition in ultrasonic vibration assisted grinding of optical glasses. Int J Adv Manuf Technol 86:1775–1784
32. Anderson D, Warkentin A, Bauer R (2011) Experimental and numerical investigations of single abrasive-grain cutting. Int J Mach Tool Manu 51:898–910